

# Grain Growth Probed by ngVLA Polarimetric Observations

Takahiro Ueda,<sup>1</sup> Satoshi Ohashi<sup>2</sup>, Akimasa Kataoka<sup>1</sup>

<sup>1</sup>National Astronomical Observatory of Japan, 2-21-1 Osawa, Mitaka-shi, Tokyo 181-8588, Japan

<sup>2</sup>RIKEN Cluster for Pioneering Research, 2-1, Hirosawa, Wako-shi, Saitama 351-0198, Japan  
takahiro.ueda@nao.ac.jp

## Abstract

ALMA polarimetric observations have revealed interesting polarization morphologies in protoplanetary disks. The polarization at millimeter wavelengths have been used for constraining dust sizes in disks since the polarization efficiency is sensitive to the dust size. However, the ALMA polarimetric observations have optical depths and spatial resolution which might be not enough to probe the dust evolution at the disk mid-plane where the planet formation occurs. We perform radiative transfer simulations with models based on the ALMA observations to derive predictions for ngVLA observations. We find that the polarization fraction at ngVLA wavelength is as high as  $\sim 4\%$  if the maximum dust size is 1 mm. If the disk is optically thick, ngVLA and ALMA traces the different heights of the disk. Therefore, by combining ngVLA and ALMA, we can constrain how much the vertical mixing is efficient and hence we can estimate the turbulence strength and dust size. Owing to its high sensitivity, ngVLA can observe the polarimetric morphology with a high spatial resolution and hence allows us to understand how dust size varies across disk substructures which might link with the planetesimal/planet formation. These results show that ngVLA will provide us new insights on how dust grains grow into larger bodies.

**Key words:** dust, extinction<sub>1</sub> — planets and satellites: formation<sub>2</sub> — protoplanetary disks<sub>3</sub>

## 1. Introduction

Dust grains are building materials of terrestrial planets and core of giant planets. In protoplanetary disks, dust grains are initially size of  $< 1 \mu\text{m}$  and stick together into mm/cm-sized grains called as pebbles. The pebbles are thought to grow into km-sized bodies called planetesimals via direct coagulation (e.g., Okuzumi et al. 2012; Kataoka et al. 2013) and/or local dust accumulation followed by hydro-dynamical instabilities (e.g., Youdin & Goodman 2005; Carrera et al. 2015; Drazkowska & Alibert 2017; Ueda et al. 2019). The planetesimals collide each other (e.g., Ida & Lin 2004) and/or accrete pebbles (e.g., Ormel & Klahr 2010; Lambrechts & Johansen 2012) and eventually form planets (Figure 1). Even though the evolution from dust to planetesimals has a key role in the planet formation, it is still unclear because dust grains are thought to radially drift quickly (Whipple 1972; Adachi et al. 1976) and are easy to fragment (e.g., Blum & Wurm 2000; Wada et al. 2013).

Polarimetric observation is one of the best ways to probe grain size evolution in protoplanetary disks. ALMA polarimetric observations have detected successfully the polarization at the millimeter wavelengths and have provided us new insights on the grain growth. In protoplanetary disks, millimeter polarization is thought to originate from self-scattering of dust thermal emission (Kataoka et al. 2015; Yang et al. 2016) and dust alignment with a magnetic and radiation field (Cho & Lazarian 2007; Guillet et al. 2020). The polarization morphology of these mechanisms are very different from each other; polarization vector is perpendicular to the disk minor axis for self-scattering and is azimuthal/radial direction for alignment. Since the polarization efficiency is sensitive to the maximum dust size  $a_{\text{max}}$ , we can constrain the dust size from the polar-

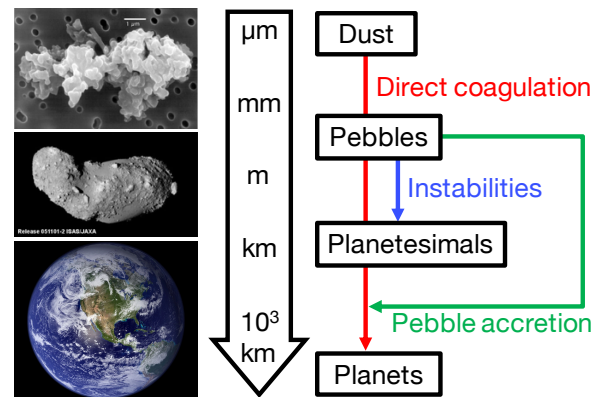


**Fig. 1.** Schematic view of size evolution of solid materials in protoplanetary disks.

ization morphology.

One of the most interesting findings from the ALMA polarimetric observations is a prevalence of  $100 \mu\text{m}$ -sized grains in disks. ALMA have revealed that many disks, regardless of their ages, show the scattering-induced polarization pattern at  $\lambda \sim 1 \text{ mm}$ , indicating that the grain growth is halted at  $\sim 100 \mu\text{m}$  in these disks even though they should contain mm-sized grains (Stephens et al. 2017; Bacciotti et al. 2018; Hull et al. 2018; Dent et al. 2019; Sadavoy et al. 2019)

However, there are some concerns on the interpretation of the ALMA polarimetric observations. One of them is an optical depth effect. Because of a sensitivity limit, current ALMA polarimetric observations focus mainly on bright disks and hence they might be optically thick at the ALMA wavelength (Ohashi et al. 2020; Ueda et al. submitted). If the disk is optically thick,

we no longer observe the disk mid-plane where large grains exist and planet formation takes place. In addition to that, the current spatial resolution for polarimetric observations is not enough to resolve substructures which have been already found with higher angular resolution observations. If disk properties changes dramatically within a small scale compared to the observing beam size, the interpretation of the polarimetric observations would need to be modified (Lin et al. 2020) Since the substructures are thought to be associated with on going planetesimal/planet formation, spatially resolved polarimetric observations on the substructures are of most importance for understanding how dust evolves into larger bodies.

Grain alignment mechanisms are still an issue even at the disk scale. First, in which scale and at which wavelengths the alignment-induced polarization dominate over self-scattering? It is believed that millimeter-wave polarization is dominated by intrinsic polarization from ellipsoidal dust grains aligned with magnetic fields down to sub-parsec scales (e.g., Girart et al. 2006). While many disks show the polarimetric pattern with the central part dominated by self-scattering at 0.9 mm, some disks show alignment-induced polarization at 3.1 mm (Kataoka et al. 2017) or at the outer part of even at 0.9 mm (Mori et al. 2019). Lopsided disks show the grain-size dependent polarimetric pattern (Ohashi et al. 2018). Furthermore, the direction of the alignment is uncertain. While the radiative torque alignment theory achieved a great success in B-field alignment in star-forming clouds, the direction of grain alignment may not be with the magnetic fields but with gas-flow or with anisotropic radiation (Tazaki et al. 2017; Kataoka et al. 2019) since dust grains in disks are much bigger than the interstellar medium and surrounded by dense gas. Phenomenological discussions on interpreting disk polarimetric pattern have shown that magnetic field direction may not be the dominant direction of intrinsic polarization (Ohashi et al. 2018; Mori et al. 2019; Yang et al. 2019; Mori & Kataoka 2020), while more fundamental discussion on microphysics of grain alignment is needed.

The “Next Generation Very Large Array” (ngVLA) will have a technical capability of the polarimetric observation at (sub-)cm wavelengths. As shown in Figure 2, the polarization due to self-scattering is sensitive to the grain size. With the current ALMA sensitivity, knowledge on polarization has developed for the wavelength of 0.9 mm, which revealed the  $\sim 150$  micron-sized dust grains. In contrast, the ngVLA wavelengths are sensitive to the dust size of  $\sim 1$  mm which is the most importance in the context of planet formation. Owing to its high sensitivity and long wavelength, the ngVLA polarimetric observations will allow us to see the polarimetric morphology at the disk mid-plane where planet formation occurs with a reasonable observation time. In this project, we perform radiative transfer simulations with models based on ALMA observations to derive predictions for ngVLA polarimetric observations. In Section 2, we investigate how vertical mixing of dust grains affect the polarization. In Section 3, we demonstrate the capability of high angular resolution polarimetric observations with ngVLA with taking the HD 163296 disk as an example. The detection limit of the polarization at ngVLA wavelength is discussed in Section 4 and conclusions are given in Section 5

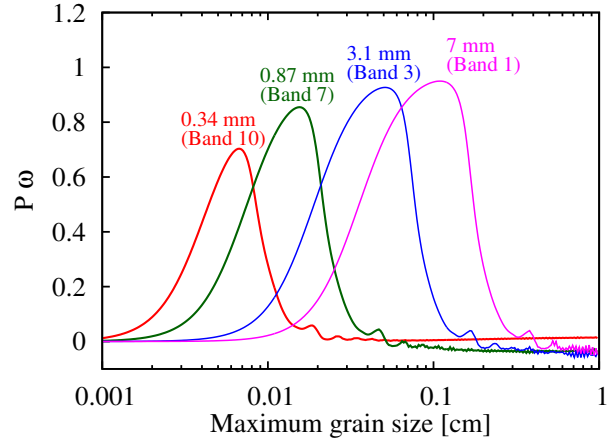


Fig. 2. The predicted polarization efficiency due to self-scattering as a function of the grain size. See Kataoka et al. (2015) for more details.

## 2. Probing vertical mixing of dust grains

As mentioned in Section 1, polarimetric observations by ALMA have provided us many insights on the dust growth. However, the disks can be optically thick at mm wavelengths and hence we cannot observe the disk mid-plane. Owing to its long observing wavelengths, ngVLA would be able to observe the disk mid-plane. We expect that by combining ALMA and ngVLA observations, we can constrain the vertical dust distribution and hence the dust size and turbulence strength. In this section, we investigate how dust settling affects the disk polarization by performing radiative transfer simulations.

### 2.1. Model

We carry out radiative transfer simulations with taking vertical dust settling and mixing into account. The model used in this section is based on the model of Ueda et al. submitted. In this subsection, we briefly summarize key points in the model and refer readers to Ueda et al. submitted for details.

In protoplanetary disks, the vertical dust distribution is determined by the equilibrium between the settling and turbulent mixing and the dust scale height can be written as (Dubrulle et al. 1995; Youdin & Lithwick 2007)

$$h_d = h_g \left( 1 + \frac{St}{\alpha_t} \frac{1 + 2St}{1 + St} \right)^{-1/2}, \quad (1)$$

where  $h_g$  is the gas scale height,  $\alpha_t$  is the strength of the turbulence and  $St$  is the normalized stopping time which is proportional to the dust radius.

At each radial grid, the vertically integrated dust size distribution is assumed to be a power-law distribution ranging from  $0.1 \mu\text{m}$  to  $a_{\text{max}}$  with a power-law index of 3.5. We consider two cases where  $a_{\text{max}} = 160 \mu\text{m}$  and 1 mm. The dust size distribution is logarithmically divided into 15 size bins per decade and Equation 1 is applied to each size bin. The radial profiles of the dust surface density and temperature are determined from the millimeter SED of the HL Tau disk within the  $\sim 20$  au and

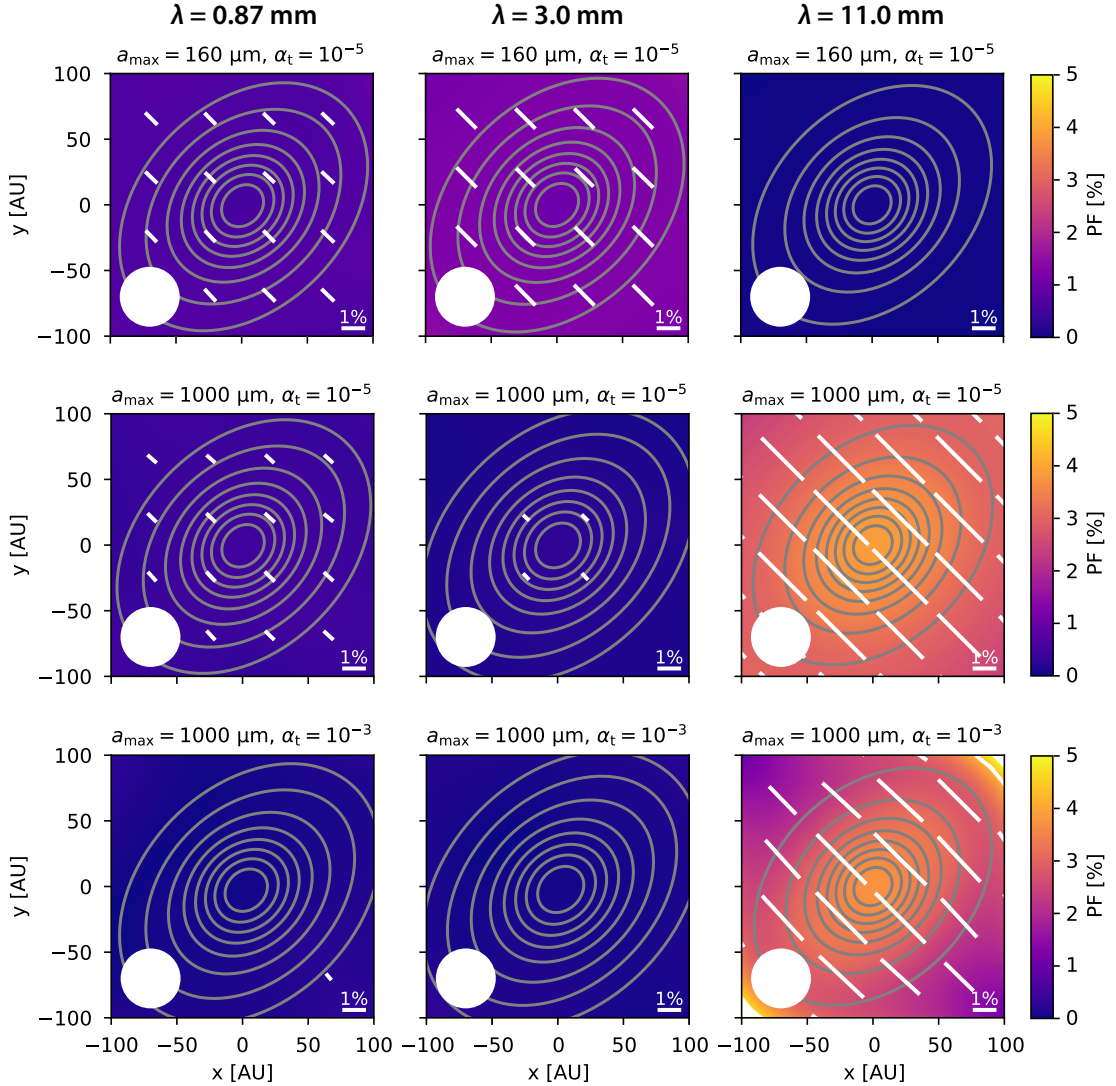


**Fig. 3.** Simulated polarization fraction of the disks with  $a_{\max} = 160 \mu\text{m}$  (top) and  $a_{\max} = 1000 \mu\text{m}$  (middle and bottom) at the observing wavelength of  $870 \mu\text{m}$  (left),  $3 \text{ mm}$  (center) and  $11 \text{ mm}$  (right). The gray solid lines denote the intensity contours linearly separated into 10 bins from the maximum to 0. The white filled circle at the bottom left in each panel denotes the observing beam size.

hence we ignore the substructures observed in the outer disk.

## 2.2. Results

Figure 3 shows the simulated polarization fraction of the model disk at different observing wavelengths. Interestingly, both models with  $a_{\max} = 160 \mu\text{m}$  and  $a_{\max} = 1000 \mu\text{m}$  predict comparable level of polarization at  $\lambda = 870 \mu\text{m}$  when  $\alpha_t = 10^{-5}$  (top and middle panels). This is because large grains are hidden in the mid-plane and we can only observe small grains at the upper layer at  $\lambda = 870 \mu\text{m}$ . As the observing wavelength increases, we can observe a layer closer to the mid-plane where the large grains reside and hence difference in the polarization fraction is more significant.

If we compare models of  $a_{\max} = 1 \text{ mm}$  with different  $\alpha_t$  (middle and bottom panels), we can see that the polarization fraction at  $\lambda = 11 \text{ mm}$  is almost the same, while only model with  $\alpha_t = 10^{-5}$  predict the polarization level observed in the

HL Tau disk at  $\lambda = 870 \mu\text{m}$ . Therefore, we can know the true dust size and turbulence strength by combining the ALMA and ngVLA polarimetric observations.

## 3. Dust size variation across the substructures

ALMA observations have revealed that many disks have gap and ring-like structures which might be associated with the formation of planets. Therefore, it is important to understand how dust size varies with the observed substructures. ngVLA will have a capability to observe the polarized emission with an angular resolution high enough to resolve some of the observed substructures. In this section, we demonstrate the capability of ngVLA high angular polarimetric observations with taking the HD 163296 disk as an example.

One big improvement is the high sensitivity observations at  $3 \text{ and } 7 \text{ mm}$  with ngVLA compared with ALMA. Polarimetric

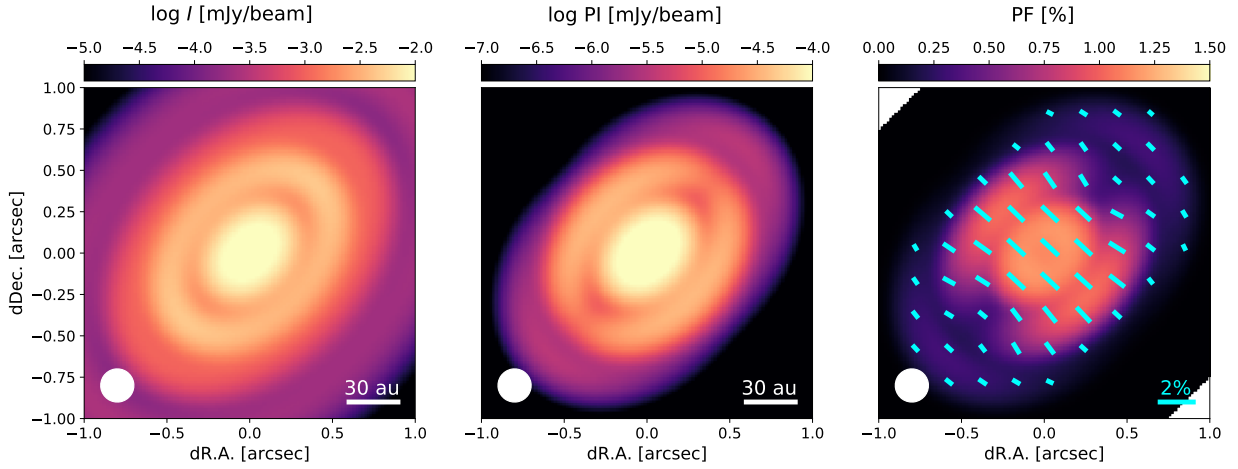


**Fig. 4.** Simulated intensity (left), polarized intensity (center) and polarization fraction (right) of the HD 163296 disk at 7 mm. The image is smoothed to the beam size of 0.2 arcsec.

substructures have been observed only at 0.9 mm, which is the currently available shortest wavelength for polarization with ALMA because sensitivity is not high enough at longer wavelengths, such as 3 mm, with spatial resolution high enough to resolve the ring and gap structures. Therefore, current analysis is limited to the brightest disks and at single band analysis. Once ngVLA reaches the spatial resolution as high as 0.1 arcsec to resolve the rings and gaps and the high sensitivity down to detecting 1% of thermal dust emission, we will be finally able to discuss the polarimetric SEDs at rings and gaps, and difference of the grain sizes between rings and gaps.

### 3.1. Model

Here, we show an example of the polarization images obtained by the radiative transfer simulations of self-scattering suitable for ngVLA observations in Figure 4. The disk is assumed to be HD 163296 because this is the only disk where the rings and gaps are spatially resolved and investigated in millimeter-wave polarization measurements so far.

Ohashi & Kataoka (2019) have investigated the grain size and dust scale height structures of the HD 163296 disk by reproducing the observed polarization features with the simulations. They suggested that the maximum grain size is  $a_{\max} \sim 140 \mu\text{m}$  in the gaps, while it becomes significantly larger or smaller in the rings. By taking into account that the ring structures are formed by pressure bumps and the grain growth proceeds, we consider the maximum grain size of 1.4 millimeter in the rings and inner part of the disk.

### 3.2. Results

Figure 4 shows the simulated images of the total intensity, polarized intensity, and polarization fraction of the HD 163296 disk at a 7 mm observing wavelength. The images are smoothed to the beam size of 0.2 arcsec.

As shown in the figure, the ring and gap structure can be imaged by the ngVLA observations. Furthermore, the polarized emission will be observed in the ring regions by ngVLA 7 mm dust continuum observations, while it was observed in the gap regions by the ALMA 0.87 mm dust continuum observations.

Thus, the observations of ngVLA together with ALMA will allow us to reveal the different grain size distributions related to the disk structure.

The polarized intensity can be detected with  $0.01 - 0.2 \mu\text{Jy beam}^{-1}$  and a beam size of 0.2 arcsec. An integration time of 4 – 5 hours on source will allow us to detect the polarization from inner 30 au with above  $3\sigma$ . Furthermore, if the beam size is as large as 0.4 arcsec, the polarized emission is detectable from the ring region with an integration time of  $\sim 10$  hours.

## 4. Sensitivity comparison

In this section, we estimate the detection limit of the polarized emission by comparing the expected noise level of ngVLA observations and the intensity profile of the HL Tau disk as an example. Figure 5 compares the radial intensity profile of the HL Tau disk at  $\lambda = 7.9$  mm observed with VLA (Carrasco-González et al. 2019) and expected noise level for an observation with 1 hr integration time by ngVLA. The observing beam size is set to be 0.1 arcsec, which is  $\sim 3$  times or more better than the typical ALMA polarimetric observations. As shown in Section 2 and 3, we expect  $\sim 1-5\%$  polarization at ngVLA wavelengths. If the polarization fraction is 1% at  $\lambda = 7.9$  mm, the polarized emission from the HL Tau disk can be detected within  $\sim 30$  au with  $> 3\sigma$  noise level. If the polarization fraction is 5%, the polarization can be detectable even at  $\sim 65$  au. With increasing the integration time and/or lowering the resolution, we would be able to observe the polarized emission more outer region.

## 5. Conclusions

We performed radiative transfer simulations with models based on the ALMA observations to derive predictions for ngVLA polarimetric observations.

First, we examine the effect of dust settling and mixing on the polarization. At the sub-mm wavelength, polarization fraction of 0.5% which is observed in the HL Tau disk, can be generated either of 100  $\mu\text{m}$ -sized and mm-sized grains be-

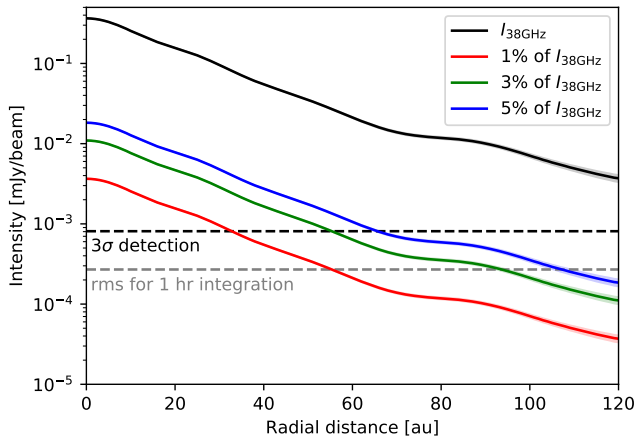


**Fig. 5.** Comparison between the intensity profile of the HL Tau disk at  $\lambda = 7.9$  mm ( $\nu = 38$  GHz) and the expected noise level of the ngVLA observation. The black solid line denotes the observed intensity profile at  $\lambda = 7.9$  mm and the uncertainty caused by the thermal noise is denoted with the translucent color (original data is from (Carrasco-González et al. 2019)). The red, green and blue solid lines denote 1%, 3% and 5% of the observed intensity, respectively. The gray and black dashed lines show the expected root mean square (rms) of the noise and  $3\times$ rms for 1 hour integration, respectively. The beam size is set to be 0.1 arcsec.

cause large grains are hidden at the mid-plane where sub-mm wavelength cannot observe. However, at the ngVLA wavelengths, owing to the low optical depth, the polarization fraction changes sensitively with the dust size and the degeneracy can be solved.

Second, we demonstrate that the high angular polarimetric observation with ngVLA allows us to constrain the dust size varying with sub-structures with taking the HD 163296 disk as an example. The observed rings and gaps in HD 163296 are expected to contain different dust population; large dust in rings and small dust in gaps. Our model predicted higher polarization fraction at innerdisk and rings and lower at gaps at the ngVLA wavelength. The spatial variation can be detected with a reasonable observing time.

Finally, we compared the observed radial intensity profile of the HL Tau disk with the expected noise level in the ngVLA observation to see the detection limit of the polarization quantitatively. We found that the polarization within  $\sim 30$  au can be detectable with 1 hr integration time if the polarization fraction is 1%. If the polarization fraction is 5%, the detectable region expands to 65 au.

These results showed that ngVLA untangles the concerns invoked from ALMA polarimetric observations and will be able to tell us how dust grains evolve into larger bodies.

## References

Adachi, I., Hayashi, C., & Nakazawa, K. 1976, *Progress of Theoretical Physics*, 56, 1756  
 Bacciotti, F., Girart, J. M., Padovani, M., et al. 2018, *ApJL*, 865, L12  
 Blum, J., & Wurm, G. 2000, *Icarus*, 143, 138  
 Carrasco-González, C., Sierra, A., Flock, M., et al. 2019, *ApJ*, 883,

71

Carrera, D., Johansen, A., & Davies, M. B. 2015, *A&A*, 579, A43  
 Cho, J., & Lazarian, A. 2007, *ApJ*, 669, 1085  
 Dent, W. R. F., Pinte, C., Cortes, P. C., et al. 2019, *MNRAS*, 482, L29  
 Drążkowska, J., & Alibert, Y. 2017, *A&A*, 608, A92  
 Dubrulle, B., Morfill, G., & Sterzik, M. 1995, *Icarus*, 114, 237  
 Girart, J. M., Rao, R., & Marrone, D. P. 2006, *Science*, 313, 812  
 Guillet, V., Girart, J. M., Maury, A. J., & Alves, F. O. 2020, *A&A*, 634, L15  
 Hull, C. L. H., Yang, H., Li, Z.-Y., et al. 2018, *ApJ*, 860, 82  
 Ida, S., & Lin, D. N. C. 2004, *ApJ*, 604, 388  
 Kataoka, A., Okuzumi, S., & Tazaki, R. 2019, *ApJL*, 874, L6  
 Kataoka, A., Tanaka, H., Okuzumi, S., & Wada, K. 2013, *A&A*, 557, L4  
 Kataoka, A., Tsukagoshi, T., Pohl, A., et al. 2017, *ApJL*, 844, L5  
 Kataoka, A., Muto, T., Momose, M., et al. 2015, *ApJ*, 809, 78  
 Lambrechts, M., & Johansen, A. 2012, *A&A*, 544, A32  
 Lin, Z.-Y. D., Li, Z.-Y., Yang, H., et al. 2020, *MNRAS*, 496, 169  
 Mori, T., & Kataoka, A. 2020, *arXiv e-prints*, arXiv:2012.01735  
 Mori, T., Kataoka, A., Ohashi, S., et al. 2019, *ApJ*, 883, 16  
 Ohashi, S., & Kataoka, A. 2019, *ApJ*, 886, 103  
 Ohashi, S., Kataoka, A., Nagai, H., et al. 2018, *ApJ*, 864, 81  
 Ohashi, S., Kataoka, A., van der Marel, N., et al. 2020, *ApJ*, 900, 81  
 Okuzumi, S., Tanaka, H., Kobayashi, H., & Wada, K. 2012, *ApJ*, 752, 106  
 Ormel, C. W., & Klahr, H. H. 2010, *A&A*, 520, A43  
 Sadavoy, S. I., Stephens, I. W., Myers, P. C., et al. 2019, *ApJS*, 245, 2  
 Stephens, I. W., Yang, H., Li, Z.-Y., et al. 2017, *ApJ*, 851, 55  
 Tazaki, R., Lazarian, A., & Nomura, H. 2017, *ApJ*, 839, 56  
 Ueda, T., Flock, M., & Okuzumi, S. 2019, *ApJ*, 871, 10  
 Wada, K., Tanaka, H., Okuzumi, S., et al. 2013, *A&A*, 559, A62  
 Whipple, F. L. 1972, in *From Plasma to Planet*, ed. A. Elvius, 211  
 Yang, H., Li, Z.-Y., Looney, L., & Stephens, I. 2016, *MNRAS*, 456, 2794  
 Yang, H., Li, Z.-Y., Stephens, I. W., Kataoka, A., & Looney, L. 2019, *MNRAS*, 483, 2371  
 Youdin, A. N., & Goodman, J. 2005, *ApJ*, 620, 459  
 Youdin, A. N., & Lithwick, Y. 2007, *Icarus*, 192, 588